JOURNAL OF MOLECULAR SPECTROSCOPY **164,** 395–415 (1994)

Rotational Spectroscopy of the CoH Radical in Its Ground $^3\Phi$ State by Far-Infrared Laser Magnetic Resonance: Determination of Molecular Parameters[1]

STUART P. BEATON,*,[2] KENNETH M. EVENSON,* AND JOHN M. BROWN†

**Time and Frequency Division, National Institute of Standards and Technology, Boulder, Colorado 80303; and †Physical Chemistry Laboratory, South Parks Road, Oxford OX1 3QZ, England*

Five rotational transitions of CoH in its ground $^3\Phi$ state have been detected by far-infrared laser magnetic resonance, three in the lowest $\Omega = 4$ component and two in the $\Omega = 3$ component. All the Zeeman transitions show an octet hyperfine pattern due to the ^{59}Co nucleus ($I = 7/2$). The much smaller proton doubling was also resolved for most transitions. The data have been fitted to experimental accuracy by an effective Hamiltonian for a molecule in an isolated $^3\Phi$ state. The electron orbital and spin g factors determined by the data confirm conclusively that the ground state of CoH is a $^3\Phi$ state. The accurate measurement of the rotational constant allows the equilibrium bond length to be determined:

$$r_e = 0.15138435(80) \text{ nm}.$$

A small Λ-type doubling was resolved in the $^3\Phi_3$ component, suggesting the proximity of a $^3\Sigma$ state among the low-lying electronic states. The cobalt hyperfine splittings have been fitted to determine magnetic dipole and electric quadrupole parameters, which are interpreted in terms of the dominant configuration description for the $^3\Phi$ ground state.

INTRODUCTION

The diatomic transition metal hydrides are of interest in a number of areas: astrophysics, molecular bonding, models for chemi-absorbed hydrogen and catalysis, and tests of ab initio wavefunctions. Hydrogen is the most abundant element in the universe, and the first row transition metals are also fairly abundant. For example, the cosmic abundance of iron is estimated to be $3 \times 10^{-3}\%$, that of cobalt $9 \times 10^{-5}\%$, and that of chromium $5 \times 10^{-5}\%$. Thus hydrides of the first row transition metals are expected to be present in stars, nebulas, and the interstellar medium. The metal hydrides CrH and FeH have already been identified in the atmospheres of several cool, M-type stars (*1–3*) by observation of their electronic spectra. It should now be possible to record far-infrared spectra of transition metal hydrides in the interstellar medium (*4*). Under the conditions expected, these spectra will consist of rotational transitions within the ground electronic state. In order to detect these hydrides in astrophysical sources both electronic and rotational ground state parameters must be precisely determined through laboratory experiments. We report here high-precision rotational parameters for CoH determined by far-infrared laser magnetic resonance (FIR LMR) spectroscopy.

[1] Supported in part by NASA Grant W15-047.

[2] Present address: Department of Chemistry, University of Denver, Denver, CO 80208.

0022-2852/94 $6.00

For many of the transition metal hydrides, a large number of low-lying electronic configurations are possible. This presents quite a challenge to ab initio theoreticians if they are to model the perturbations of the electronic states which arise accurately. For cobalt hydride, over 30 electronic states of singlet, triplet, and quintet multiplicity are expected to lie within 30 000 cm^{-1} of the ground state (*5*).

Cobalt hydride has been the subject of spectroscopic research since 1937 when Heimer (*6*) reported emission bands at 449.2 and 420.3 nm from a King furnace loaded with cobalt and hydrogen at 2400 K. He ascribed these to the (0, 0) and (1, 0) vibrational bands of the $A^3\Phi_4 \rightarrow X^3\Phi_4$ electronic transition. Klynning and Neuhaus (*7*) and Klynning and Kronekvist (*8–10*), using a King furnace in both emission and absorption, showed that the lower $\Omega = 4$ state of the 449 and 420 nm bands was the ground state, and also observed a similar transition between $\Omega = 3$ states at 455 nm. They suggested that the lower $\Omega = 3$ state was the middle spin component of the ground $^3\Phi$ electronic state; however, they did not observe the $\Omega = 2$ component. Klynning and Kronekvist (*10*) were able to determine the rotational parameters B and D for each of the three vibrational levels involved in the $\Omega = 4$–4 transition, as well as for the lower state of the $\Omega = 3$–3 transition. Due to severe perturbations they could not determine the parameters for the upper vibrational level of the $\Omega = 3$ state. Smith (*11*) also recorded several absorption bands of CoH produced in a shock tube, but did not attempt a rotational analysis. Varberg *et al.* (*12*) have recently observed six new bands of CoH in the red by laser-induced fluorescence. The transitions involved both the $\Omega = 4$ and the $\Omega = 3$ spin components of the ground state and they were able to measure the $\Omega = 4 - 3$ separation as -728 ± 3 cm^{-1}.

It was expected that the eightfold hyperfine splitting due to the ^{59}Co nucleus (abundance = 100%, $I = 7/2$) would be large enough to be observed in the optical spectrum (*7*). However, this was not the case and the splitting was first observed by Beaton *et al.* for CoH in the $^3\Phi_4$ state by far-infrared LMR spectroscopy (*13*), and then by mid-infrared CO LMR (*14*).

We report here the observation of far-infrared LMR spectra of rotational transitions of CoH in the $\Omega = 4$ and $\Omega = 3$ components of the $X^3\Phi$ state including nuclear-spin-forbidden resonances and a complete analysis of these data. In addition, many unidentified resonances have been observed; judging from the hyperfine structure they also arise from CoH, but have not yet been assigned. They are probably spectra of CoH in other low-lying electronic states.

EXPERIMENTAL DETAILS

Details of the far-infrared laser magnetic resonance spectrometer are given elsewhere (*15*). CoH was produced in a flow system by reacting atomic hydrogen with cobalt carbonyl, in the same manner we have used for producing other transition metal hydrides (*13, 16*). A microwave discharge in 200 Pa (1.5 Torr) helium with 6.5 Pa (50 mTorr) hydrogen generated the atomic hydrogen. Cobalt carbonyl vapor (either $Co_2(CO)_8$ or $CoNO(CO)_3$) was entrained in helium and carried to the reaction region. The liquid $CoNO(CO)_3$ gave the best signal-to-noise ratio, as it produced a higher vapor pressure, about 0.4 Pa (3 mTorr) in the reaction region, than did the crystalline $Co_2(CO)_8$. The optimum chemistry did not depend strongly on the He or H_2 pressures, though excess carbonyl destroyed the signal. The optimum signals in the two observed spin components did not appear to require different chemical conditions.

The details of the rotational transitions of CoH detected and assigned in the present work are given, along with the far-infrared laser lines used, in Table I. This information is summarized in Fig. 1 which shows the lowest few rotational levels in the lower two spin components of the $X\,^3\Phi$ state.

The field values at resonance were read from 0.1 T (1 kG) scans. An example of such a scan is shown in Fig. 4. The signal-to-noise ratio with a 1-sec time constant exceeded 1000 for the strongest lines. The accuracy of individual measurements is estimated as 0.3 mT.

ASSIGNMENT OF SPECTRA

The CoH molecule shows strong spin–orbit coupling in its ground state, and in some respects is a good example of Hund's case (a) coupling. The Zeeman effect is therefore close to linear, and the assignment of the transitions is straightforward. Figure 2 shows the LMR spectrum of CoH at 2557.3654 GHz (117.2 μm), in parallel (π) polarization. The field values at the centers of the hyperfine octets form a series in the ratio $\frac{1}{5}$, $\frac{1}{4}$, $\frac{1}{3}$, $\frac{1}{2}$, and $\frac{1}{1}$, from which the M_J values for both the upper and lower states are easily determined to equal 5, 4, 3, 2, and 1, respectively, and the rotational transition involved must be $J = 6 \leftarrow 5$.

The effects of uncoupling the cobalt nuclear spin from the internuclear axis is evident in Fig. 2. This is shown by the changing hyperfine spacing for the low-field lines compared with the constant spacing at higher fields. The intensities of the lines in the octet are not uniform in the low-field region, either. At higher resolution, each line shows a small doubling ($\approx$1 mT) due to the proton hyperfine splitting. The relative strength of the cobalt hyperfine interaction is shown by the ratio of the cobalt-to-proton hyperfine splitting and the high field ($\approx$200 mT) required to uncouple the cobalt nuclear spin from the internuclear axis. By comparison, the proton splitting in CrH was much weaker and completely decoupled by fields of only 10 mT (*16*).

TABLE I

Summary of the Transitions Observed in ^{59}CoH in the $v = 0$ Level of the $X\,^3\Phi$ State by Laser Magnetic Resonance

Transition		Laser Line			
Spin Component	$J' \leftarrow J''$	λ / μm	ν/MHz[a]	Lasing Gas	Pump
$^3\Phi_4$	$5 \leftarrow 4$	139.3	2 152 662.4	CD_2F_2	10R(20)
		138.3	2 167 691.2	$^{13}CH_2F_2$	9R(22)
	$6 \leftarrow 5$	117.7	2 546 495.0	CH_2F_2	9R(20)
		117.2	2 557 365.4	CH_3OD	9P(26)
	$7 \leftarrow 6$	100.8	2 973 941.15	CH_3OH	9R(14)
$^3\Phi_3$	$4 \leftarrow 3$	171.8	1 745 439.0	$^{13}CH_3OH$	10R(18)
		170.6	1 757 526.3	CH_3OH	9P(36)
	$5 \leftarrow 4$	138.3	2 167 691.2	$^{13}CH_2F_2$	9R(22)

[a] The laser frequencies are taken from the review article by Inguscio, *et al.* (23) except for the 171.8 μm line where a more reliable frequency is given by Henningsen and Peterson (25) and for the 100.8 μm line which we have recently re-measured more accurately.

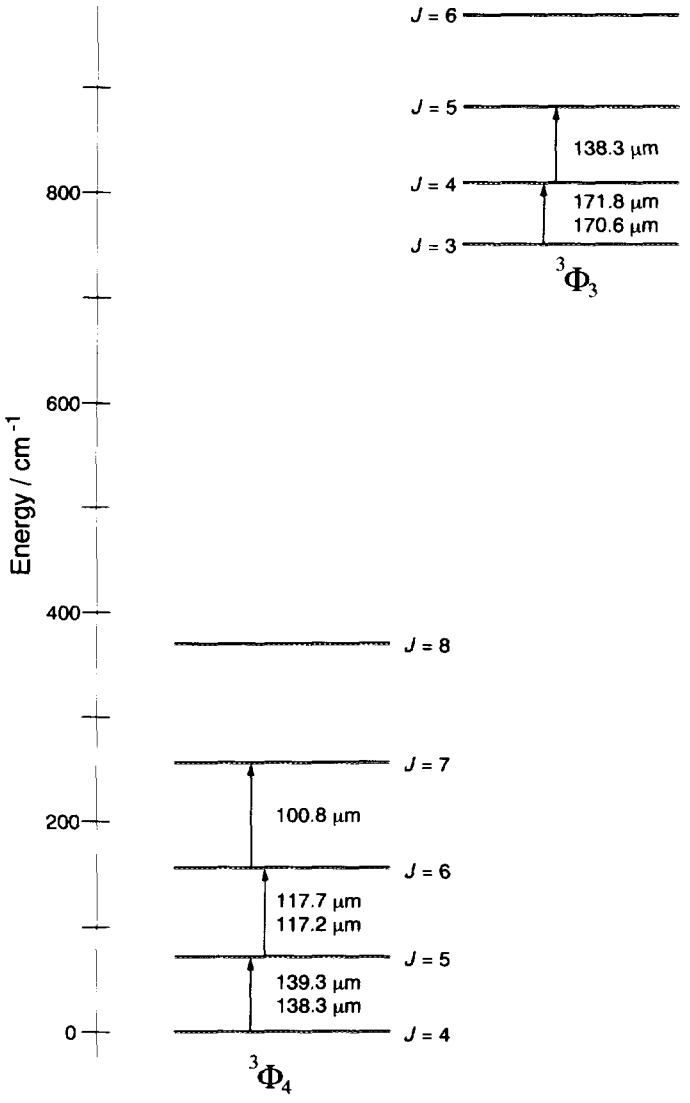

FIG. 1. An energy level diagram showing the lowest few rotational levels of the lower two spin components, with $\Omega = 4$ and 3, of the $X^3\Phi$ state of CoH. The $\Omega = 2$ component is expected to lie at an energy of approximately 1500 cm^{-1}. The rotational transitions detected in the present study are indicated by arrows. The levels of the $^3\Phi_3$ component show Λ-type doubling which is easily resolved in the far-infrared LMR spectrum.

Figure 3 shows the LMR spectrum of CoH recorded at 2167.6912 GHz (138.3 μm). In this spectrum, the signals associated with the $\Omega = 4$ ground state component are the eight lines tightly grouped at 1.7 T. The two groups of lines centered at 1.08 and 1.4 T arise from CoH in the $\Omega = 3$ component, with the Λ-doubling easily resolved. The cobalt hyperfine splitting of the $\Omega = 3$ level is almost twice that of the $\Omega = 4$ level. Another set of $\Omega = 3$ lines begins at the high-field end of the spectrum where the magnet limit of 2 T is reached.

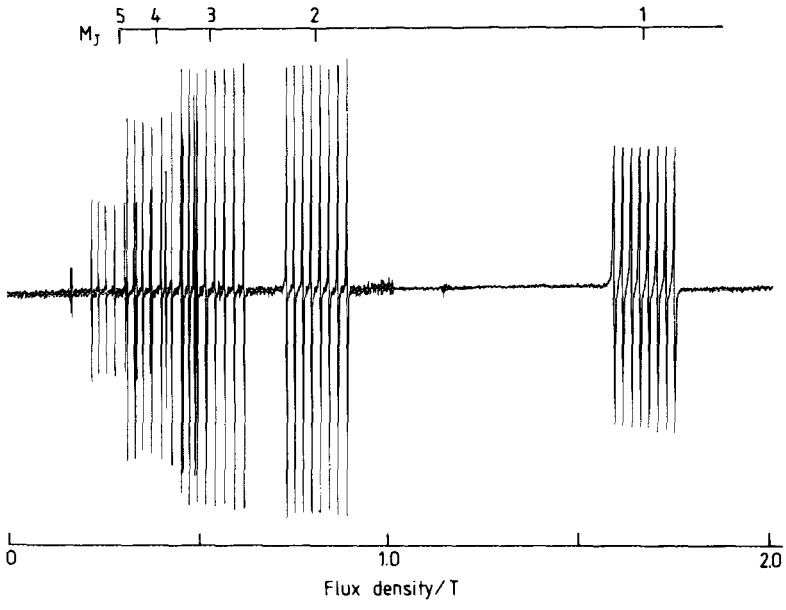

FIG. 2. The far-infrared LMR spectrum associated with the $J = 6 \leftarrow 5$ rotational transition of CoH in the $^3\Phi_4$ spin component, recorded with the 117.2-μm laser line of CH_3OD in π polarization ($\Delta M_J = 0$). The output time constant was 0.1 sec. The Zeeman effect is very close to linear and the resonance field for each Zeeman component is inversely proportional to the M_J value. Each such Zeeman component shows an octet hyperfine pattern due to the ^{59}Co nucleus (abundance = 100%, $I = 7/2$). The variation of intensity among the hyperfine patterns of the two lowest Zeeman components is a manifestation of the residual coupling of the nuclear spin to the molecular rotation. For the higher field resonances, the nuclear spin is totally decoupled from the molecular framework. It is completely quantized with respect to the applied magnetic field instead.

Figure 4 shows two sections of Fig. 3 in detail. Each section is a 0.1-T (1-kG) scan from which the resonance field values were measured. The upper section of Fig. 3 shows the spectrum associated with the $J = 5 \leftarrow 4$ transition centered at 1.08 T in the $\Omega = 3$ component; the lower section shows the spectrum associated with the $J = 5 \leftarrow 4$ transition centered at 1.7 T in the $\Omega = 4$ spin component. In the $\Omega = 3$ component the proton hyperfine splitting is about 1.9 mT and the cobalt hyperfine splitting is 46 mT, while in the $\Omega = 4$ component the proton splitting is about 1.3 mT and the cobalt splitting is 22 mT. These splittings remain constant for the different J levels within a single spin component and are very helpful in assigning transitions. The Λ-doubling is also characteristic of each spin component, being 30 mT for the $M_J = 4$ resonances in the $\Omega = 3$ component, but unresolvable in the $\Omega = 4$ component.

Table I gives a summary of the CoH transitions which have been detected and assigned. There were also a number of other resonances observed which have not been assigned but which originate from CoH, based on the presence of the eightfold splitting characteristic of the cobalt nuclear spin. Five examples of such unassigned groups of lines appear in the lower field region of Fig. 3. Table II gives a complete list of the nuclear-spin-allowed resonances which have been positively identified, along with their assignments and the residuals from the least-square fit. Table III lists the nuclear-spin-forbidden resonances observed at low magnetic field on the 171.8-μm laser line.

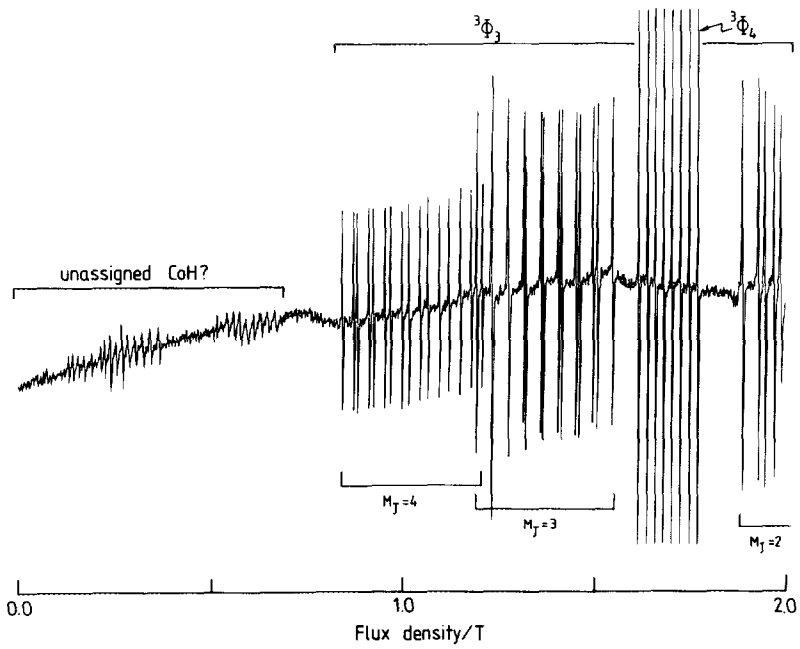

FIG. 3. The far-infrared LMR spectrum associated with the $J = 5 \leftarrow 4$ rotational transition of CoH in the $^3\Phi_3$ and $^3\Phi_4$ spin components, recorded with the 138.3-μm line in π polarization ($\Delta M_J = 0$). The eight strong signals centered at 1.7 T arise from CoH in the $\Omega = 4$ component, showing the hyperfine structure of the cobalt nucleus. The two groups of lines centered at 1.08 and 1.40 T are assigned to CoH in the $\Omega = 3$ component, with the Λ-type doubling easily resolved. The weaker groups of lines at lower field have not yet been assigned. The hyperfine structure shows that they are associated with CoH also, presumably in another low-lying electronic state which is populated in the chemical reaction.

RESULTS

The assigned LMR data for CoH were used to determine parameters of an effective Hamiltonian for a $^3\Phi$ state in a least-squares fit. The form of the Hamiltonian was taken as

$$\mathbf{H}_{\text{eff}} = \mathbf{H}_{\text{rot}} + \mathbf{H}_{\text{cd}} + \mathbf{H}_{\text{so}} + \mathbf{H}_{\text{sr}} + \mathbf{H}_{\text{ss}} + \mathbf{H}_{\text{ld}} + \mathbf{H}_{\text{hfs}} + \mathbf{H}_{\text{zeem}}, \tag{1}$$

where the various terms are (*17*)

$$\mathbf{H}_{\text{rot}} = B_v\mathbf{N}^2 \quad \text{rotational kinetic energy} \tag{2}$$

$$\mathbf{H}_{\text{cd}} = -D_v\mathbf{N}^4 \quad \text{centrifugal distortion correction} \tag{3}$$

$$\mathbf{H}_{\text{so}} = A_v L_z S_z, \quad \text{spin–orbit coupling} \tag{4}$$

$$\mathbf{H}_{\text{sr}} = \gamma_v\mathbf{N}\cdot\mathbf{S} + \gamma_{Dv}(\mathbf{N}\cdot\mathbf{S})\mathbf{N}^2 \quad \text{spin–rotation coupling} \tag{5}$$

$$\mathbf{H}_{\text{ss}} = 2\lambda_v(S_z^2 - \tfrac{1}{3}\mathbf{S}^2) \quad \text{spin–spin coupling} \tag{6}$$

$$\mathbf{H}_{\text{ld}} = \tfrac{1}{2}q_{\Phi v}(\mathbf{N}_+^6 + \mathbf{N}_-^6) \quad \Lambda\text{-type doubling} \tag{7}$$

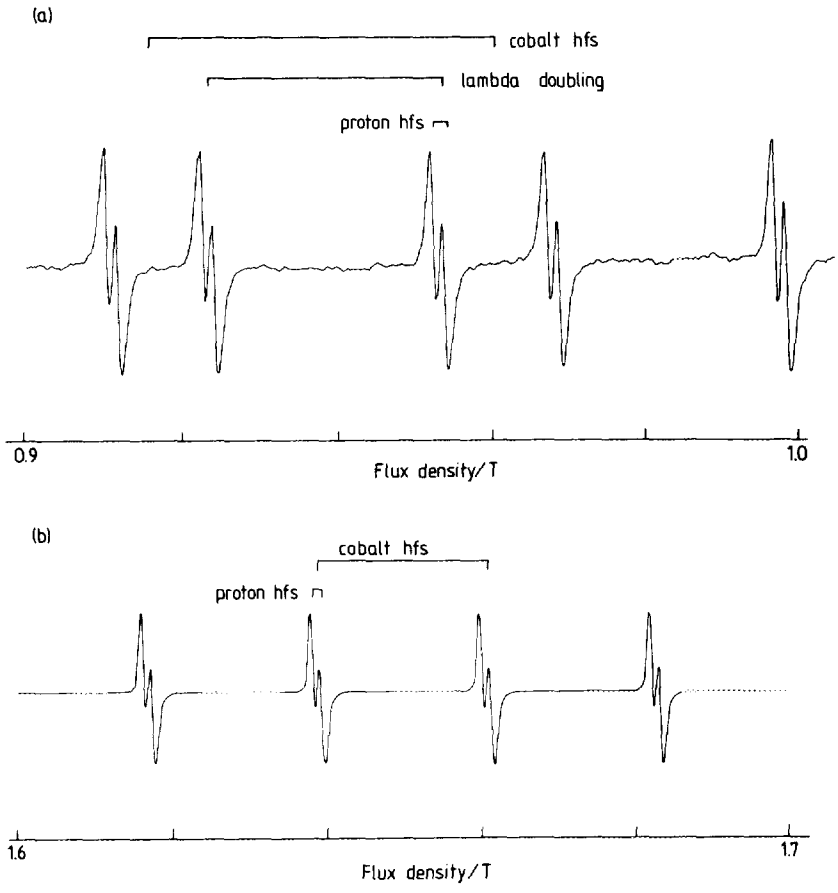

FIG. 4. Two sections of the LMR spectrum of the CoH radical in detail. Each section corresponds to a 0.1-T (1-kG) scan; magnetic field measurements of individual resonances were taken from scans of this type. Both spectra were recorded with the 138.3-μm laser line and are associated with the $J = 5 \leftarrow 4$ transition; that in (a) is for CoH in the $\Omega = 3$ spin component while that in (b) is for CoH in the $\Omega = 4$ spin component. Note that the Co hyperfine splitting is much larger than the proton hyperfine splitting and that Λ-type doubling is resolvable for the $\Omega = 3$ transitions. Also, the hyperfine splittings for both nuclei are larger in the $\Omega = 3$ component.

$$\mathbf{H}_{\text{hfs}} = aI_zL_z + b\mathbf{I}\cdot\mathbf{S} + cI_zL_z \qquad \text{magnetic hyperfine interaction} \qquad (8)$$

$$\mathbf{H}_{\text{zeem}} = (g_L + g_r)\mu_B B_0 L_Z + g_S\mu_B B_0 S_Z + g_I(B_x S_x + B_y S_y) - g_I\mu_N B_0 N_Z - g_I\mu_N B_0 I_Z \qquad \text{the Zeeman interactions.} \qquad (9)$$

Standard nomenclature has been used throughout. The rotationally dependent terms have been expressed in terms of $\mathbf{N}^2$ rather than $\mathbf{R}^2$ (*18*). The matrix representation was constructed in a Hund's case (a) basis set and is given for the first seven terms, Eqs. (2) to (8), in Table IV. Λ-type doubling was resolved for transitions in the $^3\Phi_3$ component (see Fig. 2). This splitting has been modeled by adding the term given in

TABLE II

The Assignments of Transitions Observed for CoH in the $X\,^3\Phi$ State by Far-Infrared Laser Magnetic Resonance

M_J	M_J	p'' [b]	Field (mT)	o-c [a] (MHz)	tr [c]	M_J	M_J	p'' [b]	Field (mT)	o-c [a] (MHz)	tr [c]
$\Omega = 4$, $J = 5 \leftarrow 4$, $\nu_{laser} = 2152.6624$ GHz											
$-4 \leftarrow -4$	3.5	0	780.89	6.7	18.0	$0 \leftarrow -1$	−1.5	0	1095.55	4.0	14.6
$-4 \leftarrow -4$	2.5	0	801.78	2.0	18.0	$0 \leftarrow -1$	−2.5	0	1118.33	−2.1	14.6
$-4 \leftarrow -4$	1.5	0	822.78	2.8	17.9	$0 \leftarrow -1$	−3.5	0	1140.92	1.5	14.6
$-4 \leftarrow -4$	0.5	0	844.17	3.6	17.9	$1 \leftarrow 0$	3.5	0	1460.79	1.9	10.3
$-4 \leftarrow -4$	−0.5	0	865.86	5.7	17.9	$1 \leftarrow 0$	2.5	0	1480.89	1.1	10.3
$-4 \leftarrow -4$	−1.5	0	888.05	5.2	17.9	$1 \leftarrow 0$	1.5	0	1501.69	−2.7	10.3
$-4 \leftarrow -4$	−2.5	0	910.74	1.6	17.9	$1 \leftarrow 0$	0.5	0	1522.50	−2.2	10.3
$-4 \leftarrow -4$	−3.5	0	933.33	5.1	17.9	$1 \leftarrow 0$	−0.5	0	1543.60	−0.4	10.3
$-3 \leftarrow -3$	3.5	0	1060.17	5.2	13.6	$1 \leftarrow 0$	−1.5	0	1565.40	−1.2	10.3
$-3 \leftarrow -3$	2.5	0	1081.26	6.6	13.6	$1 \leftarrow 0$	−2.5	0	1587.41	0.5	10.3
$-3 \leftarrow -3$	1.5	0	1103.44	−2.1	13.6	$1 \leftarrow 0$	−3.5	0	1610.11	−0.1	10.3
$-3 \leftarrow -3$	0.5	0	1125.63	−6.2	13.6	$-5 \leftarrow -4$	3.5	0	1811.15	3.6	8.1
$-3 \leftarrow -3$	−0.5	0	1147.61	−2.8	13.6	$-5 \leftarrow -4$	2.5	0	1835.63	5.2	8.1
$-3 \leftarrow -3$	−1.5	0	1170.10	−1.9	13.6	$-5 \leftarrow -4$	1.5	0	1860.36	5.8	8.1
$-3 \leftarrow -3$	−2.5	0	1192.88	−0.7	13.6	$-5 \leftarrow -4$	0.5	0	1885.09	7.3	8.1
$-3 \leftarrow -3$	−3.5	0	1215.77	3.1	13.6	$-5 \leftarrow -4$	−0.5	0	1910.20	6.4	8.1
$-2 \leftarrow -2$	3.5	0	1605.31	2.4	9.3	$-5 \leftarrow -4$	−1.5	0	1935.32	6.2	8.1
$-2 \leftarrow -2$	2.5	0	1626.92	2.4	9.3	$-5 \leftarrow -4$	−2.5	0	1960.40	6.7	8.1
$-2 \leftarrow -2$	1.5	0	1648.72	3.4	9.3	$-5 \leftarrow -4$	−3.5	0	1986.70	−2.2	8.1
$-2 \leftarrow -2$	0.5	0	1670.70	5.7	9.3						
$-2 \leftarrow -2$	−0.5	0	1693.17	6.4	9.3	$\Omega = 4$, $J = 5 \leftarrow 4$, $\nu_{laser} = 2167.6912$ GHz					
$-2 \leftarrow -2$	−1.5	0	1716.15	5.2	9.3	$-4 \leftarrow -4$	3.5	0	1616.27	0.7	18.0
$-2 \leftarrow -2$	−2.5	0	1739.13	6.9	9.3	$-4 \leftarrow -4$	2.5	0	1637.98	2.9	18.0
$-2 \leftarrow -2$	−3.5	0	1762.60	7.0	9.3	$-4 \leftarrow -4$	1.5	0	1659.97	2.9	18.0
$-3 \leftarrow -4$	3.5	0	482.12	10.6	28.1	$-4 \leftarrow -4$	0.5	0	1682.16	1.9	17.9
$-3 \leftarrow -4$	2.5	0	501.21	−1.3	27.9	$-4 \leftarrow -4$	−0.5	0	1704.34	3.4	17.9
$-3 \leftarrow -4$	1.5	0	520.40	0.4	27.8	$-4 \leftarrow -4$	−1.5	0	1726.82	1.6	17.9
$-3 \leftarrow -4$	0.5	0	540.09	3.9	27.7	$-4 \leftarrow -4$	−2.5	0	1749.31	1.7	17.9
$-3 \leftarrow -4$	−0.5	0	560.39	5.2	27.6	$-4 \leftarrow -4$	−3.5	0	1772.09	−1.8	17.9
$-3 \leftarrow -4$	−1.5	0	581.18	7.0	27.6	$-3 \leftarrow -4$	3.5	0	1020.40	−11.0	27.9
$-3 \leftarrow -4$	−2.5	0	602.47	7.9	27.5	$-3 \leftarrow -4$	2.5	0	1040.69	−8.7	27.8
$-3 \leftarrow -4$	−3.5	0	624.16	9.6	27.5	$-3 \leftarrow -4$	1.5	0	1061.28	−6.7	27.8
$-2 \leftarrow -3$	3.5	0	586.47	5.9	23.5	$-3 \leftarrow -4$	0.5	0	1082.26	−7.9	27.8
$-2 \leftarrow -3$	2.5	0	605.77	4.0	23.4	$-3 \leftarrow -4$	−0.5	0	1103.44	−7.5	27.7
$-2 \leftarrow -3$	1.5	0	625.36	8.2	23.4	$-3 \leftarrow -4$	−1.5	0	1125.22	−16.8	27.7
$-2 \leftarrow -3$	0.5	0	645.65	8.6	23.3	$-3 \leftarrow -4$	−2.5	0	1146.80	−14.2	27.7
$-2 \leftarrow -3$	−0.5	0	666.54	7.3	23.3	$-3 \leftarrow -4$	−3.5	0	1168.78	−16.7	27.7
$-2 \leftarrow -3$	−1.5	0	687.83	8.4	23.2	$-2 \leftarrow -3$	3.5	0	1226.32	−7.0	23.5
$-2 \leftarrow -3$	−2.5	0	710.02	−0.3	23.2	$-2 \leftarrow -3$	2.5	0	1246.90	−6.4	23.5
$-2 \leftarrow -3$	−3.5	0	732.11	4.0	23.2	$-2 \leftarrow -3$	1.5	0	1267.79	−6.5	23.5
$-1 \leftarrow -2$	3.5	0	740.81	4.8	19.0	$-2 \leftarrow -3$	0.5	0	1288.99	−7.4	23.4
$-1 \leftarrow -2$	2.5	0	760.50	4.8	19.0	$-2 \leftarrow -3$	−0.5	0	1310.28	−4.2	23.4
$-1 \leftarrow -2$	1.5	0	780.69	5.0	19.0	$-2 \leftarrow -3$	−1.5	0	1331.97	−4.3	23.4
$-1 \leftarrow -2$	0.5	0	801.48	3.4	18.9	$-2 \leftarrow -3$	−2.5	0	1353.86	−3.3	23.4
$-1 \leftarrow -2$	−0.5	0	822.68	3.6	18.9	$-2 \leftarrow -3$	−3.5	0	1376.05	−3.6	23.4
$-1 \leftarrow -2$	−1.5	0	844.27	5.7	18.9	$-1 \leftarrow -2$	3.5	0	1527.83	−1.1	19.2
$-1 \leftarrow -2$	−2.5	0	866.46	5.7	18.9	$-1 \leftarrow -2$	2.5	0	1548.63	−2.2	19.2
$-1 \leftarrow -2$	−3.5	0	889.05	7.2	18.9	$-1 \leftarrow -2$	1.5	0	1569.53	0.0	19.1
$0 \leftarrow -1$	3.5	0	991.01	1.5	14.6	$-1 \leftarrow -2$	0.5	0	1590.93	−2.1	19.1
$0 \leftarrow -1$	2.5	0	1011.10	0.4	14.6	$-1 \leftarrow -2$	−0.5	0	1612.24	2.6	19.1
$0 \leftarrow -1$	1.5	0	1031.49	1.6	14.6	$-1 \leftarrow -2$	−1.5	0	1634.14	1.2	19.1
$0 \leftarrow -1$	0.5	0	1052.38	2.3	14.6	$-1 \leftarrow -2$	−2.5	0	1656.33	−0.5	19.1
$0 \leftarrow -1$	−0.5	0	1073.77	2.5	14.6	$-1 \leftarrow -2$	−3.5	0	1678.71	−0.9	19.1

[a] The calculated transition frequency is obtained using the parameter values given in Table V.

[b] Assumed absolute parity of the lower level of the transition. A value of 0 indicates that lambda-doubling was not resolved, and therefore the relative parity could not be determined.

[c] The tuning rate, in MHz/mT, calculated using the parameters given in Table V.

[d] These lines were blended and the field position is only approximate. They were not used in the fit.

TABLE II—*Continued*

M_J	M_J	p'' [b]	Field (mT)	o-c [a] (MHz)	tr [c]	M_J	M_J	p'' [b]	Field (mT)	o-c [a] (MHz)	tr [c]
$\Omega = 4$, $J = 6 \leftarrow 5$, ν_{laser} = 2546.4950 GHz						1 ← 2	−2.5	0	1269.83	0.8	−12.3
5 ← 5	3.5	0	1088.66	1.1	−12.7	1 ← 2	−3.5	0	1292.51	0.0	−12.3
5 ← 5	2.5	0	1110.64	1.3	−12.7	0 ← 1	3.5	0	1465.39	3.0	−9.7
5 ← 5	1.5	0	1133.12	0.3	−12.7	0 ← 1	2.5	0	1485.69	1.9	−9.7
5 ← 5	0.5	0	1156.11	−1.9	−12.7	0 ← 1	1.5	0	1505.39	−7.2	−9.7
5 ← 5	−0.5	0	1179.89	−1.9	−12.8	0 ← 1	0.5	0	1527.20	2.0	−9.7
5 ← 5	−1.5	0	1204.58	1.7	−12.8	0 ← 1	−0.5	0	1548.10	0.4	−9.7
5 ← 5	−2.5	0	1229.56	0.8	−12.8	0 ← 1	−1.5	0	1569.40	0.8	−9.7
5 ← 5	−3.5	0	1255.24	0.4	−12.8	0 ← 1	−2.5	0	1590.81	0.3	−9.7
4 ← 4	3.5	0	1386.63	−1.7	−10.2	0 ← 1	−3.5	0	1612.91	4.7	−9.7
4 ← 4	2.5	0	1409.12	2.5	−10.2						
4 ← 4	1.5	0	1431.70	3.3	−10.2	$\Omega = 4$, $J = 6 \leftarrow 5$, ν_{laser} = 2557.3654 GHz					
4 ← 4	0.5	0	1454.48	1.9	−10.2	5 ← 5	3.5	0	222.18	3.1	−11.7
4 ← 4	−0.5	0	1477.69	0.5	−10.2	5 ← 5	2.5	0	239.68	2.6	−11.3
4 ← 4	−1.5	0	1501.69	2.8	−10.2	5 ← 5	1.5	0	259.57	1.5	−11.0
4 ← 4	−2.5	0	1525.80	1.8	−10.2	5 ← 5	0.5	0	282.67	3.8	−10.8
4 ← 4	−3.5	0	1550.20	−0.7	−10.2	5 ← 5	−0.5	0	308.47	−2.0	−10.8
3 ← 3	3.5	0	1887.98	1.4	−7.6	5 ← 5	−1.5	0	338.97	−1.8	−11.1
3 ← 3	2.5	0	1910.60	4.1	−7.6	5 ← 5	−2.5	0	374.36	−1.6	−11.8
3 ← 3	1.5	0	1933.02	3.4	−7.6	5 ← 5	−3.5	0	415.26	−2.2	−13.3
3 ← 3	0.5	0	1955.90	4.2	−7.6	4 ← 4	3.5	0	313.47	−1.9	−9.9
3 ← 3	−0.5	0	1979.00	4.7	−7.6	4 ← 4	2.5	0	333.17	−1.6	−9.8
3 ← 3	−1.5	0	2002.20	4.1[d]	−7.6	4 ← 4	1.5	0	354.06	−7.0	−9.7
3 ← 3	−2.5	0	2025.80	4.6[d]	−7.6	4 ← 4	0.5	0	378.06	−0.4	−9.7
3 ← 3	−3.5	0	2050.00	7.7[d]	−7.6	4 ← 4	−0.5	0	403.16	−2.1	−9.8
4 ← 5	3.5	0	662.94	0.8	−19.8	4 ← 4	−1.5	0	430.46	−1.7	−9.9
4 ← 5	2.5	0	683.83	−4.3	−19.8	4 ← 4	−2.5	0	459.65	−1.4	−10.1
4 ← 5	1.5	0	706.52	8.2	−19.8	4 ← 4	−3.5	0	490.65	0.1	−10.4
4 ← 5	0.5	0	729.12	0.3	−19.8	3 ← 3	3.5	0	455.85	−1.5	−7.6
4 ← 5	−0.5	0	753.01	−1.1	−19.8	3 ← 3	2.5	0	475.55	−8.8	−7.5
4 ← 5	−1.5	0	778.09	1.3	−19.9	3 ← 3	1.5	0	498.44	−0.3	−7.5
4 ← 5	−2.5	0	804.18	3.7	−20.1	3 ← 3	0.5	0	520.84	−3.6	−7.5
4 ← 5	−3.5	0	830.97	−0.7	−20.2	3 ← 3	−0.5	0	544.64	−4.5	−7.5
3 ← 4	3.5	0	776.40	0.0	−17.4	3 ← 3	−1.5	0	569.73	−3.6	−7.6
3 ← 4	2.5	0	797.09	−5.8	−17.3	3 ← 3	−2.5	0	596.13	−0.1	−7.6
3 ← 4	1.5	0	819.48	5.9	−17.3	3 ← 3	−3.5	0	622.62	−3.0	−7.7
3 ← 4	0.5	0	841.57	0.2	−17.3	2 ← 2	3.5	0	733.69	−2.1	−5.1
3 ← 4	−0.5	0	864.66	−0.4	−17.4	2 ← 2	2.5	0	755.18	−1.7	−5.0
3 ← 4	−1.5	0	888.25	−4.8	−17.4	2 ← 2	1.5	0	777.17	−1.7	−5.0
3 ← 4	−2.5	0	913.04	−0.8	−17.5	2 ← 2	0.5	0	799.66	−1.9	−5.0
3 ← 4	−3.5	0	938.23	−2.3	−17.5	2 ← 2	−0.5	0	822.26	−4.2	−5.0
2 ← 3	3.5	0	927.43	−1.0	−14.8	2 ← 2	−1.5	0	845.95	−3.5	−5.0
2 ← 3	2.5	0	948.22	−2.1	−14.8	2 ← 2	−2.5	0	870.14	−2.5	−5.1
2 ← 3	1.5	0	969.51	−3.5	−14.8	2 ← 2	−3.5	0	894.73	−1.7	−5.1
2 ← 3	0.5	0	991.41	−3.3	−14.8	1 ← 1	3.5	0	1589.49	−1.4	−2.4
2 ← 3	−0.5	0	1014.10	0.9	−14.8	1 ← 1	2.5	0	1611.80	−2.0	−2.4
2 ← 3	−1.5	0	1036.89	−0.8	−14.8	1 ← 1	1.5	0	1633.90	−3.1	−2.4
2 ← 3	−2.5	0	1060.17	−2.8	−14.9	1 ← 1	0.5	0	1656.80	−2.4	−2.4
2 ← 3	−3.5	0	1084.16	−1.6	−14.9	1 ← 1	−0.5	0	1679.28	−2.7	−2.4
1 ← 2	3.5	0	1140.32	−1.3	−12.3	1 ← 1	−1.5	0	1701.76	−2.8	−2.4
1 ← 2	2.5	0	1160.81	−3.6	−12.3	1 ← 1	−2.5	0	1724.25	−2.8	−2.4
1 ← 2	1.5	0	1181.79	−4.3	−12.3	1 ← 1	−3.5	0	1746.93	−2.2	−2.4
1 ← 2	0.5	0	1203.68	1.8	−12.3	2 ← 3	3.5	0	189.58	3.2	−14.2
1 ← 2	−0.5	0	1225.26	−0.1	−12.3	2 ← 3	2.5	0	206.78	−2.0	−13.9
1 ← 2	−1.5	0	1247.35	0.0	−12.3	2 ← 3	1.5	0	226.98	0.6	−13.9

Eq. (7) to the Hamiltonian; the two terms in parentheses on the right-hand side connect states with $\Delta\Lambda = \Delta\Omega = -6$ and $+6$, respectively.

Varberg *et al.* (*12*) have measured the separation between the $\Omega = 3$ and 4 components of the ground state of CoH as $-728\ cm^{-1}$. This energy difference corresponds

TABLE II—*Continued*

M_J	M_J	p'' [b]	Field (mT)	o-c [a] (MHz)	tr [c]	M_J	M_J	p'' [b]	Field (mT)	o-c [a] (MHz)	tr [c]
2 ← 3	0.5	0	249.58	1.6	−14.0	Ω = 4, J = 7 ← 6, ν_{laser} = 2973.94115 GHz					
2 ← 3	−0.5	0	274.47	2.4	−14.3	6 ← 6	3.5	0	972.61	9.0	−9.5
2 ← 3	−1.5	0	300.37	−7.4	−14.7	6 ← 6	2.5	0	994.70	8.2	−9.5
2 ← 3	−2.5	0	328.07	−2.2	−14.8	6 ← 6	1.5	0	1017.39	7.0	−9.5
2 ← 3	−3.5	0	354.86	−5.0	−14.6	6 ← 6	0.5	0	1040.89	7.3	−9.5
1 ← 2	3.5	0	256.17	1.2	−12.3	6 ← 6	−0.5	0	1064.98	7.1	−9.6
1 ← 2	2.5	0	274.47	1.9	−12.2	6 ← 6	−1.5	0	1089.96	8.9	−9.6
1 ← 2	1.5	0	294.17	1.8	−12.1	6 ← 6	−2.5	0	1115.25	7.3	−9.6
1 ← 2	0.5	0	314.67	−5.6	−12.1	6 ← 6	−3.5	0	1141.34	6.8	−9.6
1 ← 2	−0.5	0	337.07	−4.8	−12.2	5 ← 5	3.5	0	1186.81	5.6	−8.0
1 ← 2	−1.5	0	360.46	−3.7	−12.2	5 ← 5	2.5	0	1209.00	5.8	−8.0
1 ← 2	−2.5	0	384.46	−3.0	−12.2	5 ← 5	1.5	0	1231.49	4.6	−8.0
1 ← 2	−3.5	0	408.16	−8.6	−12.1	5 ← 5	0.5	0	1254.88	6.7	−8.0
0 ← 1	3.5	0	349.86	−4.7	−9.8	5 ← 5	−0.5	0	1278.46	6.6	−8.0
0 ← 1	2.5	0	368.26	−3.7	−9.8	5 ← 5	−1.5	0	1302.34	5.0	−8.0
0 ← 1	1.5	0	387.46	−3.5	−9.8	5 ← 5	−2.5	0	1326.93	5.2	−8.0
0 ← 1	0.5	0	407.26	−5.4	−9.7	5 ← 5	−3.5	0	1352.11	6.3	−8.0
0 ← 1	−0.5	0	428.06	−4.6	−9.7	4 ← 4	3.5	0	1508.57	8.1	−6.4
0 ← 1	−1.5	0	449.45	−3.9	−9.7	4 ← 4	2.5	0	1530.58	6.8	−6.4
0 ← 1	−2.5	0	471.25	−3.5	−9.7	4 ← 4	1.5	0	1553.09	6.6	−6.4
0 ← 1	−3.5	0	493.44	−1.9	−9.6	4 ← 4	0.5	0	1576.10	7.5	−6.4
−1 ← 0	3.5	0	505.74	−4.8	−7.3	4 ← 4	−0.5	0	1599.11	6.2	−6.4
−1 ← 0	2.5	0	523.94	−3.9	−7.2	4 ← 4	−1.5	0	1622.82	7.4	−6.4
−1 ← 0	1.5	0	542.74	−2.2	−7.2	4 ← 4	−2.5	0	1646.63	7.1	−6.4
−1 ← 0	0.5	0	561.73	−2.4	−7.2	4 ← 4	−3.5	0	1670.91	7.8	−6.4
−1 ← 0	−0.5	0	581.23	−1.6	−7.2	4 ← 5	3.5	0	660.11	0.2	−13.5
−1 ← 0	−1.5	0	600.73	−3.1	−7.2	4 ← 5	2.5	0	681.00	−0.7	−13.5
−1 ← 0	−2.5	0	620.92	−1.5	−7.2	4 ← 5	1.5	0	702.89	0.7	−13.5
−1 ← 0	−3.5	0	641.12	−0.9	−7.1	4 ← 5	0.5	0	725.39	−0.9	−13.5
6 ← 5	3.5	0	658.01	−0.5	−5.6	4 ← 5	−0.5	0	748.68	−3.1	−13.5
6 ← 5	2.5	0	680.51	0.7	−5.6	4 ← 5	−1.5	0	773.17	−0.5	−13.6
6 ← 5	1.5	0	703.40	−1.0	−5.5	4 ← 5	−2.5	0	798.36	0.3	−13.6
6 ← 5	0.5	0	727.09	−3.6	−5.5	4 ← 5	−3.5	0	824.35	0.7	−13.7
6 ← 5	−0.5	0	752.58	−1.7	−5.5	3 ← 4	3.5	0	762.67	1.4	−12.0
6 ← 5	−1.5	0	778.87	−1.0	−5.5	3 ← 4	2.5	0	783.27	0.1	−12.0
6 ← 5	−2.5	0	805.76	−2.9	−5.5	3 ← 4	1.5	0	804.56	−0.5	−11.9
6 ← 5	−3.5	0	834.15	−2.6	−5.6	3 ← 4	0.5	0	826.65	1.0	−12.0
−2 ← −1	3.5	0	830.65	−2.3	−4.7	3 ← 4	−0.5	0	849.15	−0.2	−12.0
−2 ← −1	2.5	0	848.05	−2.0	−4.6	3 ← 4	−1.5	0	872.24	−1.7	−12.0
−2 ← −1	1.5	0	865.64	−1.7	−4.6	3 ← 4	−2.5	0	895.93	−3.4	−12.0
−2 ← −1	0.5	0	883.34	−1.4	−4.6	3 ← 4	−3.5	0	920.62	−0.3	−12.1
−2 ← −1	−0.5	0	900.83	−2.6	−4.6	2 ← 3	3.5	0	895.13	1.0	−10.4
−2 ← −1	−1.5	0	918.93	−1.3	−4.6	2 ← 3	2.5	0	915.33	−1.4	−10.4
−2 ← −1	−2.5	0	935.82	−5.7	−4.6	2 ← 3	1.5	0	936.22	−1.5	−10.4
−2 ← −1	−3.5	0	954.72	−0.8	−4.6	2 ← 3	0.5	0	957.51	−2.4	−10.4
5 ← 4	3.5	0	1298.55	−2.3	−3.0	2 ← 3	−0.5	0	979.41	−1.7	−10.4
5 ← 4	2.5	0	1323.64	−3.2	−3.0	2 ← 3	−1.5	0	1001.70	−1.8	−10.4
5 ← 4	1.5	0	1349.42	−3.7	−3.0	2 ← 3	−2.5	0	1024.29	−3.4	−10.4
5 ← 4	0.5	0	1376.10	−3.2	−3.0	2 ← 3	−3.5	0	1047.79	−0.1	−10.4
5 ← 4	−0.5	0	1403.08	−3.5	−3.0	1 ← 2	3.5	0	1074.17	−2.1	−8.8
5 ← 4	−1.5	0	1430.57	−4.0	−3.0	1 ← 2	2.5	0	1094.36	−1.4	−8.8
5 ← 4	−2.5	0	1458.96	−3.6	−3.0	1 ← 2	1.5	0	1114.75	−2.0	−8.8
5 ← 4	−3.5	0	1487.76	−3.8	−3.0	1 ← 2	0.5	0	1135.74	−0.4	−8.8
						1 ← 2	−0.5	0	1156.73	−1.6	−8.8
						1 ← 2	−1.5	0	1178.32	−0.4	−8.8

to $(3A - 2\lambda + 4\gamma - 8B)$ in terms of the parameters in the effective Hamiltonian. We have arbitrarily chosen to constrain the spin–spin coupling parameter λ to zero in our fit so that the measurement by Varberg *et al.* corresponds to a value for A of -221.5 cm^{-1} (or -6640 GHz). The centrifugal distortion correction to A was not included

TABLE II—*Continued*

M_J	M_J	p'' [b]	Field (mT)	o-c [a] (MHz)	tr [c]
1 ← 2	−2.5	0	1200.41	2.4	−8.8
1 ← 2	−3.5	0	1222.39	1.5	−8.8
0 ← 1	3.5	0	1332.02	−3.1	−7.2
0 ← 1	2.5	0	1351.71	−3.3	−7.2
0 ← 1	1.5	0	1371.80	−2.3	−7.2
0 ← 1	0.5	0	1391.88	−3.1	−7.2
0 ← 1	−0.5	0	1412.77	0.4	−7.2
0 ← 1	−1.5	0	1433.26	−0.5	−7.2
0 ← 1	−2.5	0	1454.25	0.7	−7.2
0 ← 1	−3.5	0	1475.16	−0.1	−7.2
−1 ← 0	3.5	0	1736.06	−6.9	−5.6
−1 ← 0	2.5	0	1755.05	−7.8	−5.6
−1 ← 0	1.5	0	1774.43	−7.3	−5.6
−1 ← 0	0.5	0	1794.02	−6.3	−5.6
−1 ← 0	−0.5	0	1813.51	−6.5	−5.6
−1 ← 0	−1.5	0	1833.09	−6.9	−5.6
−1 ← 0	−2.5	0	1853.16	−5.1	−5.6
−1 ← 0	−3.5	0	1873.18	−4.2	−5.6
Ω = 3, J = 4 ← 3, ν_{laser} = 1745.4390 GHz					
−1 ← −1	3.5	1	277.25	−1.1	4.4
−1 ← −1	3.5	−1	292.40	3.6[d]	4.4
−1 ← −1	2.5	1	305.74	−1.3	4.2
−1 ← −1	2.5	−1	321.94	1.1	4.3
−1 ← −1	1.5	1	337.74	−1.0	4.1
−1 ← −1	1.5	−1	354.54	0.7	4.2
−1 ← −1	0.5	1	373.93	−1.2	4.0
−1 ← −1	0.5	−1	390.93	0.9	4.1
−1 ← −1	−0.5	1	414.68	−1.6	4.0
−1 ← −1	−0.5	−1	431.43	2.0	4.1
−1 ← −1	−1.5	1	460.22	−1.2	4.1
−1 ← −1	−1.5	−1	477.12	1.2	4.1
−1 ← −1	−2.5	1	511.21	−1.8	4.2
−1 ← −1	−2.5	−1	527.71	0.4	4.2
−1 ← −1	−3.5	1	566.90	−1.3	4.4
−1 ← −1	−3.5	−1	582.90	0.3	4.4
−2 ← −2	3.5	1	76.20	0.7[d]	9.2
−2 ← −2	3.5	−1	83.88	1.3	9.2
−2 ← −2	2.5	1	93.47	−0.8	8.2
−2 ← −2	2.5	−1	102.07	0.0	8.2
−2 ← −2	1.5	1	114.47	−1.1	7.0
−2 ← −2	1.5	−1	124.37	−0.2	7.2
−2 ← −2	0.5	1	142.47	−1.6	6.3
−2 ← −2	0.5	−1	153.37	−0.8	6.6
−2 ← −2	−0.5	1	180.86	−0.9	6.5
−2 ← −2	−0.5	−1	191.36	1.4	6.7
−2 ← −2	−1.5	1	228.55	0.1	7.0
−2 ← −2	−1.5	−1	238.25	2.7	7.1
−2 ← −2	−2.5	1	282.85	−1.2	7.7
−2 ← −2	−2.5	−1	291.50	3.5[d]	7.7
−2 ← −2	−3.5	1	341.15	−2.2	8.3
−2 ← −2	−3.5	−1	349.45	0.2	8.3
−3 ← −3	3.5	1	24.50	−1.0	16.9
−3 ← −3	3.5	−1	28.60	2.0	16.4
−3 ← −3	2.5	1	31.59	0.5	10.7
−3 ← −3	2.5	−1	37.69	3.2	11.6
−3 ← −3	1.5	1	42.99	−0.3	7.4
−3 ← −3	1.5	−1	51.48	2.5	8.7
−3 ← −3	0.5	1	68.78	0.5	7.9
−3 ← −3	0.5	−1	77.60	−1.3[d]	8.6
−3 ← −3	−0.5	1	106.77	−0.4	9.1
−3 ← −3	−0.5	−1	114.47	−0.6	9.4
−3 ← −3	−1.5	1	151.50	88.6[d]	10.2
−3 ← −3	−1.5	−1	158.87	1.2	10.3
−3 ← −3	−2.5	1	202.45	−2.3	11.1
−3 ← −3	−2.5	−1	208.55	1.3	11.1
−3 ← −3	−3.5	1	255.75	0.9	11.8
−3 ← −3	−3.5	−1	261.75	1.2	11.8
Ω = 3, J = 4 ← 3, ν_{laser} = 1757.5263 GHz					
−3 ← −3	3.5	1	927.34	−1.7	13.1
−3 ← −3	3.5	−1	932.83	−2.3	13.1
−3 ← −3	2.5	1	964.53	−3.7	13.0
−3 ← −3	2.5	−1	970.12	−5.2	13.0
−3 ← −3	1.5	1	1002.51	1.4	13.0
−3 ← −3	1.5	−1	1007.91	2.6	13.0
−3 ← −3	0.5	1	1042.30	−0.1	12.9
−3 ← −3	0.5	−1	1047.90	−1.2	12.9
−3 ← −3	−0.5	1	1083.58	−4.5	12.9
−3 ← −3	−0.5	−1	1088.98	−3.0	12.9
−3 ← −3	−1.5	1	1125.45	−1.0	12.9
−3 ← −3	−1.5	−1	1131.05	−2.0	12.9
−3 ← −3	−2.5	1	1168.93	−3.6	12.9
−3 ← −3	−2.5	−1	1174.03	1.9	12.9
−3 ← −3	−3.5	1	1212.80	2.7	12.9
−3 ← −3	−3.5	−1	1218.40	1.6	12.9
−2 ← −2	3.5	1	1444.36	2.9	8.9
−2 ← −2	3.5	−1	1452.25	4.2	8.9
−2 ← −2	2.5	1	1483.66	0.1	8.8
−2 ← −2	2.5	−1	1491.67	0.5	8.8
−2 ← −2	1.5	1	1523.37	2.7	8.8
−2 ← −2	1.5	−1	1531.38	3.2	8.8
−2 ← −2	0.5	1	1564.58	1.1	8.8
−2 ← −2	0.5	−1	1572.59	1.7	8.8
−2 ← −2	−0.5	1	1606.30	3.9	8.8
−2 ← −2	−0.5	−1	1614.40	3.8	8.8
−2 ← −2	−1.5	1	1649.51	2.4	8.8
−2 ← −2	−1.5	−1	1657.70	1.4	8.8
−2 ← −2	−2.5	1	1693.77	0.2	8.8
−2 ← −2	−2.5	−1	1701.56	2.7	8.8
−2 ← −2	−3.5	1	1738.53	2.0	8.8
−2 ← −2	−3.5	−1	1746.63	1.7	8.8
−2 ← −3	3.5	−1	568.58	3.0	20.2
−2 ← −3	2.5	−1	602.37	1.6	19.9
−2 ← −3	1.5	1	634.36	0.1	19.8
−2 ← −3	1.5	−1	637.96	0.1	19.8
−2 ← −3	0.5	1	671.64	−1.0	19.6
−2 ← −3	0.5	−1	675.34	−2.4	19.6
−2 ← −3	−0.5	1	710.32	3.1	19.5
−2 ← −3	−0.5	−1	714.02	2.0	19.5

in our fit because its effect on the molecular energy levels is the same as that of the spin–rotation constant γ.

The hyperfine splitting due to the proton was very much smaller than the ^{59}Co hyperfine splitting and only just resolved in the spectra (see Fig. 4). In order to simplify

TABLE II—*Continued*

M_J	M_I	p'' [b]	Field (mT)	o-c [a] (MHz)	tr [c]	M_J	M_I	p'' [b]	Field (mT)	o-c [a] (MHz)	tr [c]
−2 ← −3	−1.5	1	751.40	−9.0	19.5	0 ← −1	−3.5	1	1384.40	−3.9	11.3
−2 ← −3	−1.5	−1	754.10	9.6	19.5	0 ← −1	−3.5	−1	1390.39	−0.5	11.3
−2 ← −3	−2.5	1	793.27	−8.2	19.4						
−2 ← −3	−2.5	−1	797.07	−10.8	19.4	Ω = 3, J = 5 ← 4, ν_{laser} = 2167.6912 GHz					
−2 ← −3	−3.5	1	836.45	−7.1	19.4	4 ← 4	3.5	1	841.22	−3.3	−8.4
−2 ← −3	−3.5	−1	839.95	−3.8	19.4	4 ← 4	3.5	−1	870.81	−1.2	−8.4
−1 ← −2	3.5	1	754.30	−5.8	15.7	4 ← 4	2.5	1	880.90	−1.2	−8.3
−1 ← −2	3.5	−1	758.59	−2.0	15.7	4 ← 4	2.5	−1	910.69	1.2	−8.4
−1 ← −2	2.5	1	790.18	−8.5	15.6	4 ← 4	1.5	1	922.99	−0.4	−8.3
−1 ← −2	2.5	−1	794.77	−8.9	15.6	4 ← 4	1.5	−1	952.68	0.4	−8.3
−1 ← −2	1.5	1	827.01	−0.7	15.5	4 ← 4	0.5	1	967.58	−1.3	−8.3
−1 ← −2	1.5	−1	831.46	1.5	15.5	4 ← 4	0.5	−1	997.47	1.4	−8.3
−1 ← −2	0.5	1	866.20	−4.5	15.5	4 ← 4	−0.5	1	1015.06	−1.7	−8.4
−1 ← −2	0.5	−1	870.55	−0.5	15.5	4 ← 4	−0.5	−1	1044.85	1.1	−8.4
−1 ← −2	−0.5	1	906.56	−2.3	15.4	4 ← 4	−1.5	1	1065.84	0.5	−8.4
−1 ← −2	−0.5	−1	910.88	2.4	15.4	4 ← 4	−1.5	−1	1095.13	1.2	−8.4
−1 ← −2	−1.5	1	948.52	−1.3	15.4	4 ← 4	−2.5	1	1118.91	−4.2	−8.5
−1 ← −2	−1.5	−1	953.17	−1.7	15.4	4 ← 4	−2.5	−1	1148.00	−2.0	−8.6
−1 ← −2	−2.5	1	992.11	−3.2	15.4	4 ← 4	−3.5	1	1176.08	−1.5	−8.7
−1 ← −2	−2.5	−1	996.71	−2.8	15.4	4 ← 4	−3.5	−1	1205.07	4.5	−8.7
−1 ← −2	−3.5	1	1036.30	6.7	15.4	3 ← 3	3.5	1	1190.77	−1.8	−6.4
−1 ← −2	−3.5	−1	1040.80	8.6	15.4	3 ← 3	3.5	−1	1230.45	4.4	−6.4
0 ← −1	3.5	1	1090.48	3.5	11.4	3 ← 3	2.5	1	1231.65	−0.1	−6.4
0 ← −1	3.5	−1	1096.57	5.3	11.4	3 ← 3	2.5	−1	1270.93	3.0	−6.4
0 ← −1	2.5	1	1128.55	−0.4	11.3	3 ← 3	1.5	1	1274.13	1.3	−6.3
0 ← −1	2.5	−1	1134.65	1.6	11.3	3 ← 3	1.5	−1	1312.80	0.2	−6.3
0 ← −1	1.5	1	1168.03	−4.5	11.3	3 ← 3	0.5	1	1317.50	−2.4	−6.3
0 ← −1	1.5	−1	1174.03	−1.2	11.3	3 ← 3	0.5	−1	1356.67	−0.3	−6.4
0 ← −1	0.5	1	1207.71	4.9	11.3	3 ← 3	−0.5	1	1363.27	−1.7	−6.4
0 ← −1	0.5	−1	1214.00	5.1	11.3	3 ← 3	−0.5	−1	1402.14	−1.0	−6.4
0 ← −1	−0.5	1	1250.28	−2.6	11.3	3 ← 3	−1.5	1	1410.54	−2.3	−6.4
0 ← −1	−0.5	−1	1256.28	0.9	11.3	3 ← 3	−1.5	−1	1449.61	0.5	−6.4
0 ← −1	−1.5	1	1292.85	5.6	11.3	3 ← 3	−2.5	1	1459.81	−1.1	−6.4
0 ← −1	−1.5	−1	1299.15	5.7	11.3	3 ← 3	−2.5	−1	1498.63	1.3	−6.4
0 ← −1	−2.5	1	1338.03	−0.1	11.3	3 ← 3	−3.5	1	1510.73	−0.2	−6.5
0 ← −1	−2.5	−1	1344.02	3.5	11.3	3 ← 3	−3.5	−1	1549.05	0.6	−6.5

the analysis, we have fitted the Hamiltonian to the average flux density of the proton doublets and neglected this hyperfine splitting. The hyperfine parameters which we have chosen to determine for ^{59}Co are a, b, and $(b + c)$ (*19*).

For a molecule in a Hund's case (a) $^{2S+1}\Lambda_\Omega$ state the combination of these parameters which describes the hyperfine splitting in first order is

$$h_\Omega = a\Lambda + \tfrac{1}{2}(b + c)\Sigma. \tag{10}$$

Small systematic trends in the residuals for transitions within the $^3\Phi_3$ component suggested the need for a J-dependent correction to this term. We have modeled this effect by adding a term of the form

$$h_{3D}3[F(F + 1) - J(J + 1) - I(I + 1)]/2 \tag{11}$$

to the diagonal matrix elements with $\Omega = 3$. This expansion has the same form as the diagonal matrix elements for the h_Ω term, multiplied by $J(J + 1)$.

The basis set used for the matrix representation of the Hamiltonian, including Zeeman effects, was truncated without loss of accuracy at $\Delta J = \pm 1$. The fit of the data presented some difficulty. The fit proceeded smoothly up to the point where all

TABLE III

The Assignments of Nuclear-Spin-Forbidden Transitions Observed in the 171.8-μm Spectrum of CoH

M_J	M_J	p'' [b]	Field (mT)	o-c [a] (MHz)	tr [c]
$\Omega = 3, J = 4 \leftarrow 3, \nu_{laser} = 1745.4390$ GHz					
$-4 \leftarrow -3$	$3.5 \leftarrow 2.5$	1	312.24	−2.5	5.2
$-4 \leftarrow -3$	$3.5 \leftarrow 2.5$	−1	325.74	−1.8	5.3
$-4 \leftarrow -3$	$2.5 \leftarrow 1.5$	1	365.04	−2.5	5.3
$-4 \leftarrow -3$	$2.5 \leftarrow 1.5$	−1	378.04	−0.7	5.4
$-4 \leftarrow -3$	$1.5 \leftarrow 0.5$	1	422.28	−0.9	5.5
$-4 \leftarrow -3$	$1.5 \leftarrow 0.5$	−1	434.98	0.2	5.5
$-4 \leftarrow -3$	$0.5 \leftarrow -0.5$	1	483.38	0.2	5.7
$-4 \leftarrow -3$	$0.5 \leftarrow -0.5$	−1	495.57	1.6	5.8
$-4 \leftarrow -3$	$-0.5 \leftarrow -1.5$	1	547.80	−1.2	6.0
$-4 \leftarrow -3$	$-0.5 \leftarrow -1.5$	−1	559.70	−0.9	6.0
$-4 \leftarrow -3$	$-1.5 \leftarrow -2.5$	1	613.70	1.4	6.2
$-4 \leftarrow -3$	$-1.5 \leftarrow -2.5$	−1	625.10	1.8	6.2
$-4 \leftarrow -3$	$-2.5 \leftarrow -3.5$	1	681.68	0.6	6.5
$-4 \leftarrow -3$	$-2.5 \leftarrow -3.5$	−1	692.27	3.4	6.5
$0 \leftarrow -1$	$2.5 \leftarrow 3.5$	1	35.90	1.3	9.3
$0 \leftarrow -1$	$2.5 \leftarrow 3.5$	−1	42.99	3.6	10.1
$0 \leftarrow -1$	$1.5 \leftarrow 2.5$	1	55.28	−0.1	8.1
$0 \leftarrow -1$	$1.5 \leftarrow 2.5$	−1	63.08	3.2	9.2
$0 \leftarrow -1$	$0.5 \leftarrow 1.5$	1	89.08	0.3	10.7
$0 \leftarrow -1$	$0.5 \leftarrow 1.5$	−1	95.38	0.9	11.7
$1 \leftarrow 0$	$2.5 \leftarrow 3.5$	1	141.00	54.2[d]	6.8
$1 \leftarrow 0$	$2.5 \leftarrow 3.5$	−1	151.00	57.2[d]	6.8
$1 \leftarrow 0$	$1.5 \leftarrow 2.5$	1	168.77	−0.9	6.7
$1 \leftarrow 0$	$1.5 \leftarrow 2.5$	−1	178.86	2.3	6.8
$1 \leftarrow 0$	$0.5 \leftarrow 1.5$	1	201.00	2.4[d]	7.0
$1 \leftarrow 0$	$0.5 \leftarrow 1.5$	−1	211.21	2.0	7.0
$1 \leftarrow 0$	$-0.5 \leftarrow 0.5$	1	234.95	−0.5	7.6
$1 \leftarrow 0$	$-0.5 \leftarrow 0.5$	−1	244.05	2.0	7.5

[a] The calculated transition frequency is obtained using the parameter values given in Table V.

[b] Assumed absolute parity of the lower level of the transition. A value of 0 indicates that lambda-doubling was not resolved, and therefore the relative parity could not be determined.

[c] The tuning rate, in MHz/mT, calculated using the parameters given in Table V.

[d] These lines were blended and the field position is only approximate. They were not used in the fit.

the $\Omega = 4$ and the $\Omega = 3$, $J = 4 \leftarrow 3$ data were included. For this data set, the standard deviation of the fit was less than 9 MHz. However, the parameters derived from this least-squares fit predicted the $\Omega = 3$, $J = 5 \leftarrow 4$ transitions to lie 490 MHz higher in frequency than observed. The explanation for this discrepancy lies in the rather large difference in the centrifugal correction parameter D for the $\Omega = 4$ and $\Omega = 3$ components: for $\Omega = 4$, $D = 4.15 \times 10^{-4}$ cm^{-1}, and for $\Omega = 3$, $D = 5.25 \times 10^{-4}$ cm^{-1} (*10*). The spin–rotation parameter γ in the effective Hamiltonian allows the difference of the effective B values in the two spin components to be adjusted. The difference in the two D values can therefore be modeled by introducing γ_D, the centrifugal distortion of the spin–rotation interaction. With the addition of this parameter, the complete

TABLE IV

The Matrix Representation of the Effective Hamiltonian for a $^3\Phi$ State in a Hund's Case (a) Basis Set

	$\|^3\Phi_4\rangle$	$\|^3\Phi_3\rangle$	$\|^3\Phi_2\rangle$
$\langle^3\Phi_4\|$	$3A+2\gamma+\frac{2}{3}\lambda+B(x-6)$ $-D\{(x-6)^2+2(x-12)\}$ $+\gamma_D x$	$-\sqrt{2(x-12)}\{(B-\frac{1}{2}\gamma)$ $-D(2x-4)$ $-\frac{1}{2}\gamma_D(x-2)\}$	$-\sqrt{(x-12)(x-6)}\{2D+\gamma_D$ $\mp\frac{1}{2}q_\Phi x(x-2)\}$
$\langle^3\Phi_3\|$		$-2\gamma-\frac{4}{3}\lambda+B(x+2)$ $-D\{(x+2)^2+4(x-9)\}$ $-\gamma_D(4x-14)$ $\pm\frac{1}{2}q_\Phi x(x-2)(x-6)$	$-\sqrt{2(x-6)}\{(B-\frac{1}{2}\gamma)$ $-D(2x+8)$ $-\frac{1}{2}\gamma_D(x+10)\}$
$\langle^3\Phi_2\|$			$-3A-4\gamma+\frac{2}{3}\lambda+B(x+6)$ $-D\{(x+6)^2+2(x-6)\}$ $-\gamma_D(5x+18)$

For brevity, x is defined as $J(J+1)$. The terms are defined in eqns. 2 to 8

data set was fitted very satisfactorily, the final standard deviation of the fit being 4.0 MHz when each data point was given equal weight.

In total, 522 resonances from the $\Omega = 4$ and $\Omega = 3$ spin components of the $X\,^3\Phi$ state of CoH were measured and assigned. Of these, 11 resonances were blended or beyond the linear range of the magnet, leaving 511 lines in the least-squares fit. The values of the parameters determined in the fit are given in Table V, together with their standard deviations and correlation coefficients. The residuals of the fit are given in Tables II and III.

DISCUSSION

We have observed transitions between the lowest rotational levels of the CoH radical in two spin components of its ground electronic state. These measurements have been modeled to within experimental error by an effective Hamiltonian for a $^3\Phi$ state and values have been determined for several molecular parameters (see Table V). Where comparison is possible, the values obtained in the present work are consistent with, but much more accurate than, those determined in earlier studies. Care must be taken to compare the same quantities. For example, all the studies of the electronic spectrum of CoH (*8–10, 12*) have fitted the rotational levels of each spin component to effective rotational parameters:

$$F_\Omega(J) = B_{\text{eff}}[J(J+1) - \Omega^2] - D_{\text{eff}}[J(J+1) - \Omega^2]^2. \qquad (12)$$

These parameters can be related to those of the effective Hamiltonian used in our analysis and that of Lipus *et al.* (*14*) by treating the Hund's case (a) matrix represen-

TABLE V

Molecular Parameters for ^{59}CoH in Its $X\,^3\Phi$ State, Determined in a Least-Squares Fit of the Far-Infrared Laser Magnetic Resonance Data

Parameter	Value Determined		Correlation
	MHz	cm^{-1}	Coefficient κ_i[a]
B_0	219 259.6 (20) [b]	7.313 713 (67)	1.4×10^4
D_0	16.3521 (96)	$5.4545\ (32) \times 10^{-4}$	1.2×10^3
A_0	-6 640 000 [c]	-221.5 [c]	
γ_0	-36 378 (110)	-1.2134 (37)	1.5×10^4
γ_D	130.07 (40)	0.004 339 (13)	4.0×10^3
q_Φ	0.0166 68 (81)	$5.560\ (27) \times 10^{-7}$	1.0
a	621.01 (21)	0.020 714 6 (70)	3.2
$(b+c)$	-320.08 (76)	-0.010 677 (25)	2.6
b	136.2 (60)	0.004 54 (20)	1.3
h_{3D}	2.541 (45)	$8.477\ (15) \times 10^{-5}$	1.4
eq_0Q	-92.5 (47)	-0.003 09 (16)	1.0
g_S	1.942 42 (26)		11.9
g_l	1.025 775 (88)		20.6
g_r	-0.020 689 (61)		12.1
g_s	0.0631 (30)		11.4
g_n	1.322 [d]		

[a] The correlation coefficient $\kappa_i = (\chi^{-1})_{ii}$, where χ is the matrix of correlation coefficients.

[b] The number in parentheses gives the 1σ error estimate, in units of the last quoted decimal place.

[c] Parameter constrained to this value from the optical spectrum (*12*) in the least-squares fit.

[d] Parameter constrained to this value (*25*) in the least-squares fit.

tation to second-order perturbation theory and comparing coefficients of $J(J+1)$ and $J^2(J+1)^2$. To within experimental accuracy, the effective parameters are given by

$$\Omega = 4: \quad B_{\text{eff}} = B + 2(B - \tfrac{1}{2}\gamma)^2/(3A + 2\lambda + 4\gamma - 8B) + \gamma_D - 22D_{\text{eff}} \tag{13}$$

$$D_{\text{eff}} = D + 8(B - \tfrac{1}{2}\gamma)(D + \tfrac{1}{4}\gamma_D)/(3A + 2\lambda + 4\gamma - 8B) \tag{14}$$

$$\Omega = 3: \quad B_{\text{eff}} = B - 8(B - \tfrac{1}{2}\gamma)^3/[3A + 2\lambda + 4\gamma - 8B)(3A - 2\lambda + 2\gamma - 4B)] - 4\gamma_D - 26D_{\text{eff}} \tag{15}$$

$$D_{\text{eff}} = D - 32(B - \tfrac{1}{2}\gamma)^2(D + \tfrac{1}{4}\gamma_D)/[(3A + 2\lambda + 4\gamma - 8B)(3A - 2\lambda + 2\gamma - 4B)]. \tag{16}$$

The notation is standard and is given, for example, in the paper by Brown *et al.* (*17*). When the appropriate values from Table V are substituted in these formulas, values for the effective rotational parameters are obtained which agree well with those of earlier workers, as shown in Table VI.

Our value for the rotational constant B_0, combined with the value for α_e (0.21974 $\pm$ 0.00002 cm^{-1}) determined from the infrared spectrum by Lipus *et al.* (*14*), enables us to calculate a value for the equilibrium rotational constant:

TABLE VI

Comparison of Effective Rotational Parameters in cm^{-1} for ^{59}CoH in the $v = 0$ Level of Its $X\,^3\Phi$ State

Parameter [a]	Klynning and Kronekvist (10)	Varberg *et al.* (12)	Lipus *et al.* (14)	Present work
$B_{\Omega=4}$	7.138 (2)	7.13630 (15)	7.13707 (11)	7.13680 (16)
$10^4 D_{\Omega=4}$	4.15 (15)	3.983 (9)	4.26 (2)	4.0354 (67)
$B_{\Omega=3}$	7.279 [b]	—	—	7.27450 (13)
$10^4 D_{\Omega=3}$	5.25 [b]	—	—	5.3899 (34)

[a] The effective rotational parameters are defined in eqn. (13) through (16).

[b] Error estimates not given.

$$B_e = 7.423583(77)\ cm^{-1}. \tag{17}$$

This value allows a determination of the equilibrium bond length for CoH in its ground $^3\Phi$ state,

$$r_e = 0.15138435(80)\ nm, \tag{18}$$

where the estimated 1σ error is purely statistical. The true uncertainty in this value is larger than this estimate, arising from neglect of nonlinear terms in the vibrational dependence of B_v. The value for r_e given here is in reasonable agreement with that determined by Klynning and Kronekvist (*8*) from CoD ($r_e = 0.15175$ nm).

An important result of the present study is that we are able to establish the ground state of CoH as $^3\Phi$ beyond any doubt. The ground state has always been assumed to be of $^3\Phi$ symmetry, from the earliest work by Heimer (*6*). In a molecular orbital description, the $^3\Phi$ state arises from the configuration $\sigma^2(3d\sigma)^2(3d\delta)^3(3d\pi)^3$ where the bonding σ orbital can be considered as a combination of the $4s$ orbital on the Co atom and the $1s$ orbital on the H atom. This description is supported by a very recent ground state ab initio calculation by Freindorf *et al.* (*5*). Further evidence for the assignment of the ground state as $^3\Phi$ was provided by the experimental identification of the associated $\Omega = 3$ spin component (*9, 12*). In our work, we were able to determine accurate values for the electron spin and orbital g factors, $g_S = 1.94242\ (26)$ and $g_L = 1.025775\ (88)$. These values are very close to 2.002 and 1.000, the values which would be expected if the state were a pure $^3\Phi$ state. To the extent that these numbers agree, the ground state of CoH can be described as a $^3\Phi$ state. In reality, there are small but significant differences which give a measure of the degree of contamination of the $^3\Phi$ state by other low-lying states which perturb it. Not enough is known about these other states at the moment to allow us to pursue the interpretation of the g factors. Nonetheless, there is further valuable information on the electronic structure of CoH in these parameters.

The highest spin component of the $X\,^3\Phi$ state of CoH, with $\Omega = 2$, has not yet been observed. Using the parameters determined in our fit (Table V), the frequency of the lowest rotational transition in the $^3\Phi_2$ component ($J = 3 \leftarrow 2$) is calculated to be 1336 GHz. Since this transition is the fastest tuning in this spin component, a number of laser lines with frequencies close to this value were used in an LMR experiment in an attempt to detect it. Although some of these laser lines give signals which can be attributed to CoH (based on the appearance of hyperfine octets), we have not assigned

them to the $^3\Phi_2$ component, since they do not have the expected hyperfine splittings or tuning rates. There are several factors which conspire to make the detection of CoH in the $^3\Phi_2$ component very difficult. From the parameters in Table V, this spin component is expected to lie 1400 to 1500 cm^{-1} above the ground $^3\Phi_4$ component. In our experiments, where the sample is at nearly room temperature, the Boltzmann population factor for a level at this energy is 0.001, which means a signal to noise ratio of less than 10 for the strongest resonances. Furthermore, the magnitude of the Λ-type doubling of levels in the $^3\Phi_2$ component cannot be reliably predicted from the observed doubling in the $^3\Phi_3$ component, except to state that it should be considerably larger; consequently, the frequency region in which to search for $^3\Phi_2$ transitions is not well determined. These factors are further compounded in an LMR experiment because the transitions are expected to tune very slowly; the maximum first-order tuning rate ($g_J M_J \mu_B$ for a π resonance) in the $^3\Phi_2$ level is only 9.2 MHz/mT ($J = 2$, $M_J = 2$), compared to 56 MHz/mT in the $^3\Phi_4$ level ($J = 4$, $M_J = 4$). A very close coincidence with the laser frequency is therefore required and there are rather few laser lines in the anticipated frequency region. The slow tuning characteristic also causes the resonances to be undermodulated which further reduces the signal intensity. Finally, it may well be that we have searched near the wrong frequencies to observe these signals. Since the $^3\Phi_2$ component lies higher in energy than its two counterparts and has a lower Ω value, it is likely to be perturbed more strongly by other electronic states. If this is the case, predictions which are based on an unperturbed $^3\Phi$ state are likely to be wildly wrong.

Looking in closer detail at the molecular parameters in Table V, we see that the value for the effective spin–rotation parameter, γ, is large (-1.2134 cm^{-1}), about one-sixth of the rotational constant. This suggests heavy mixing with nearby $^3\Delta$ or $^3\Gamma$ states. Of the two possibilities, the former is much more likely. The recent ab initio calculation by Freindorf *et al.* (*5*) suggests that there is a low-lying $^3\Delta$ state; it is derived from the ground $^3\Phi$ state by a one-electron promotion and is estimated to lie 3700 cm^{-1} above it. The lowest $^3\Gamma$ state is calculated to lie much higher in energy, at about 25 000 cm^{-1}. If it is the $^3\Delta$ state which significantly mixes with the ground state, the $^3\Phi_4$ component will be unaffected in first order since the mixing involves spin–orbit coupling. The $^3\Phi_3$ component on the other hand will be perturbed and this interaction could well be the cause of the large values for both γ and γ_D.

This interpretation can be tested by making an estimate of γ for CoH in the $X\,^3\Phi$ state. An expression for the second-order (dominant) contribution to γ has been given by Brown *et al.* (*18*). With the assumption that single-configuration descriptions of the $^3\Phi$ and $^3\Delta$ states are valid,

$$X\,^3\Phi\colon (3d\sigma)^2(3d\pi)^3(3d\delta)^3(4s + 1s)^2$$

$$^3\Delta\colon (3d\sigma)^1(3d\pi)^4(3d\delta)^3(4s + 1s)^2$$

and that the Cocentered molecular orbitals are well described by atomic orbitals, then

$$\gamma^{(2)} = -3\sqrt{2}B\zeta/(E_\Phi - E_\Delta). \tag{19}$$

Taking values for the atomic spin–orbit coupling constant ζ of 530 cm^{-1} (*20*) and for $(E_\Phi - E_\Delta)$ of -3700 cm^{-1}, we find that this mixing makes a contribution of -2.22 cm^{-1} to the spin–rotation parameter. Given the sweeping approximations made in the calculation, the agreement with the experimental value of -1.21 cm^{-1} is quite

good. At the very least, it tells us that there is nothing bizarre about the large magnitude of γ in this case.

Another interesting feature of the molecular parameter set is the nonzero value for the Λ-type doubling parameter, q_Φ. It is very unusual for Λ-doubling to be observed for a molecule in a Φ state. The observation of such doubling in the present case implies that there is a $^{2S+1}\Sigma$ state in the vicinity which causes Λ-type doubling with Π and Δ states acting as intermediaries. According to the ab initio calculations of Freindorf *et al.* (*5*), there is a very low-lying $^3\Sigma^-$ state about 1200 cm^{-1} above the $^3\Phi$ state, and also $^5\Sigma^-$ and $^3\Sigma^-$ states at energies of 5300 and 11 300 cm^{-1}, respectively. Any or all of these states could cause the Λ-doubling, but the lowest is the most likely.

Finally, Table V shows that we have determined all the major magnetic and electric hyperfine parameters of the ^{59}Co nucleus for CoH in the ground $^3\Phi$ state. The three combinations of hyperfine parameters given in Table V are those which are best determined from the fit of the data for CoH, which conforms closely to a Hund's case (a) limit. For interpretation, it is better to derive the three parameters which have the most direct physical significance. These are the nuclear spin–orbit coupling parameter (a), the Fermi contact parameter (b_F), and the nuclear spin–electron spin dipolar coupling constant (c). The calculated values for these parameters are given in Table VII. The nuclear spin–orbit parameter can be used to determine the expectation value of the operator $\sum_i r_i^{-3}$, where the summation is over the electrons which are responsible for the orbital angular momentum. The value obtained is 3.322×10^{31} m^{-3}, compared with the theoretical value of 4.528×10^{31} m^{-3} for an electron in a $3d$ atomic orbital on Co (*21*). This shows that the $3d\pi$ and $3d\delta$ molecular orbitals in CoH are similar to $3d$ atomic orbitals but are slightly more diffuse.

The reliability of the set of hyperfine parameters in Table VII can be judged from the value of the electron density at the nucleus, $\sum_i \langle \delta(\mathbf{r}_i) \rangle_s$, derived from the Fermi contact parameter b_F. This is small and negative, precisely in line with expectation from the ground state electronic configuration of $(3d\sigma)^2 (3d\pi)^3 (3d\delta)^3 \sigma^2$. Since the open-shell electrons are in orbitals with nodal planes at the Co nucleus, the electron density at the nucleus is zero to first order. The small negative deviation from zero is caused by spin-polarization effects, i.e., configuration interaction (*22*). Finally, we come to the dipole–dipole coupling parameter, c, which depends on the expectation value of the operator $\sum_i (3\cos^2\theta_i - 1)/r_i^{-3}$, where the summation is now carried out

TABLE VII

^{59}Co Magnetic and Electronic Hyperfine Parameters and Related Quantities for CoH in Its $X\,^3\Phi$ State

Parameter	Value
a / MHz	621.01 (21)[a]
b_F / MHz	-15.9 (86)
c / MHz	-456.3 (78)
eq_0Q / MHz	-92.5 (47)
$\langle r_i^{-3} \rangle_s$ / m^{-3}	3.3222 (11) × 10^{-31}
$\langle \delta(r_i) \rangle_s$ / m^{-3}	-1.01 (55) × 10^{24}
$\langle (3\cos^2\theta_i - 1)/r_i^{-3} \rangle_s$ / m^{-3}	-1.626 (92) × 10^{31}

[a] The number in parentheses gives the 1σ error estimate of the experimental uncertainty, in units of the last quoted decimal place.

TABLE VIII

The Predicted Zero-Field Transition Frequencies for the LMR Transitions Detected in the $\Omega = 4$ and $\Omega = 3$ Spin Components of the Ground $^3\Phi$ State of CoH

Transition F [a]	p'' [b]	Frequency (GHz)	Line Strength	Transition F [a]	p'' [b]	Frequency (GHz)	Line Strength
$\Omega = 4, J = 5 \leftarrow 4$				$6\frac{1}{2} \leftarrow 5\frac{1}{2}$	-1	1743.4550	2.35
$8\frac{1}{2} \leftarrow 7\frac{1}{2}$	0	2136.5266	2.95		1	1743.5263	2.35
$7\frac{1}{2} \leftarrow 6\frac{1}{2}$	0	2137.0750	2.38	$5\frac{1}{2} \leftarrow 4\frac{1}{2}$	-1	1744.2005	1.72
$6\frac{1}{2} \leftarrow 5\frac{1}{2}$	0	2137.5291	1.88		1	1744.2718	1.72
$5\frac{1}{2} \leftarrow 4\frac{1}{2}$	0	2137.8858	1.46	$4\frac{1}{2} \leftarrow 3\frac{1}{2}$	-1	1744.7647	1.20
$4\frac{1}{2} \leftarrow 3\frac{1}{2}$	0	2138.1427	1.10		1	1744.8360	1.20
$3\frac{1}{2} \leftarrow 2\frac{1}{2}$	0	2138.2977	0.81	$3\frac{1}{2} \leftarrow 2\frac{1}{2}$	-1	1745.1441	0.78
$2\frac{1}{2} \leftarrow 1\frac{1}{2}$	0	2138.3494	0.58		1	1745.2154	0.78
$1\frac{1}{2} \leftarrow \frac{1}{2}$	0	2138.2967	0.40	$2\frac{1}{2} \leftarrow 1\frac{1}{2}$	-1	1745.3362	0.46
$\Omega = 4, J = 6 \leftarrow 5$					1	1745.4075	0.46
$9\frac{1}{2} \leftarrow 8\frac{1}{2}$	0	2561.0408	5.14	$1\frac{1}{2} \leftarrow 0\frac{1}{2}$	-1	1745.3391	0.21
$8\frac{1}{2} \leftarrow 7\frac{1}{2}$	0	2561.3818	4.31		1	1745.4104	0.21
$7\frac{1}{2} \leftarrow 6\frac{1}{2}$	0	2561.6682	3.57	$\Omega = 3, J = 5 \leftarrow 4$			
$6\frac{1}{2} \leftarrow 5\frac{1}{2}$	0	2561.8988	2.93	$8\frac{1}{2} \leftarrow 7\frac{1}{2}$	1	2175.7934	5.23
$5\frac{1}{2} \leftarrow 4\frac{1}{2}$	0	2562.0724	2.38		-1	2176.0401	5.23
$4\frac{1}{2} \leftarrow 3\frac{1}{2}$	0	2562.1882	1.91	$7\frac{1}{2} \leftarrow 6\frac{1}{2}$	1	2176.3004	4.22
$3\frac{1}{2} \leftarrow 2\frac{1}{2}$	0	2562.2456	1.52		-1	2176.5470	4.22
$2\frac{1}{2} \leftarrow 1\frac{1}{2}$	0	2562.2440	1.21	$6\frac{1}{2} \leftarrow 5\frac{1}{2}$	1	2176.7179	3.34
$\Omega = 4, J = 7 \leftarrow 6$					-1	2176.9646	3.34
$10\frac{1}{2} \leftarrow 9\frac{1}{2}$	0	2983.7492	6.93	$5\frac{1}{2} \leftarrow 4\frac{1}{2}$	1	2177.0448	2.59
$9\frac{1}{2} \leftarrow 8\frac{1}{2}$	0	2983.9794	5.96		-1	2177.2915	2.59
$8\frac{1}{2} \leftarrow 7\frac{1}{2}$	0	2984.1750	5.10	$4\frac{1}{2} \leftarrow 3\frac{1}{2}$	1	2177.2797	1.96
$7\frac{1}{2} \leftarrow 6\frac{1}{2}$	0	2984.3355	4.34		-1	2177.5264	1.96
$6\frac{1}{2} \leftarrow 5\frac{1}{2}$	0	2984.4605	3.66	$3\frac{1}{2} \leftarrow 2\frac{1}{2}$	1	2177.4216	1.44
$5\frac{1}{2} \leftarrow 4\frac{1}{2}$	0	2984.5496	3.08		-1	2177.6683	1.44
$4\frac{1}{2} \leftarrow 3\frac{1}{2}$	0	2984.6024	2.58	$2\frac{1}{2} \leftarrow 1\frac{1}{2}$	1	2177.4699	1.02
$3\frac{1}{2} \leftarrow 2\frac{1}{2}$	0	2984.6185	2.18		-1	2177.7166	1.02
$\Omega = 3, J = 4 \leftarrow 3$				$1\frac{1}{2} \leftarrow 0\frac{1}{2}$	1	2177.4240	0.71
$7\frac{1}{2} \leftarrow 6\frac{1}{2}$	-1	1742.5327	3.11		-1	2177.6707	0.71
	1	1742.6040	3.11				

[a] Hyperfine structure arising from ^{59}Co nucleus. Each of these lines will be split by about 10 MHz by the proton hyperfine splitting.

[b] Assumed absolute parity of the lower level of the transition. A value of 0 indicates that lambda-doubling was not resolved, and therefore the relative parity could not be determined. There is a lambda-type doubling of a few megahertz on each transitionin the $\Omega = 4$ component.

over the electrons responsible for the unpaired spin angular momentum. The value determined from our work is given in Table VII. For a pure d orbital, the integral over angular coordinates of $(3\cos^2\theta - 1)$ is equal to $-4/7$ for a $d\delta$ orbital and $+2/7$ for a $d\pi$ orbital (*21*). If the electron configuration given above is a good description of the ground state wavefunction for CoH, the expectation value for $\sum_i (3\cos^2\theta_i - 1)$ would be $-2/7$ using pure $3d$ orbitals. The ratio of $\langle (3\cos^2\theta_i - 1)/r_i^3 \rangle_s$ to $\langle 1/r_i^3 \rangle_l$ determined experimentally is -0.489, rather different from -0.286 $(-2/7)$,

although it has the correct sign. This discrepancy is most likely attributable to a slight polarization of the $3d$ orbitals in the π and δ molecular orbitals.

The parameters determined from the laser magnetic resonance data (Table V) allow us to calculate the frequency of the observed rotational transitions in the absence of an external magnetic field. Table VIII gives the results, which include the effects of the cobalt hyperfine splitting and, for the $\Omega = 3$ spin component, the Λ-doubling. The estimated uncertainty in the predicted values is 0.7 MHz. The calculated linestrength of each transition, which is independent of the population factors and of the molecular dipole moment (*4*), is also given in the table. The frequencies given in Table VIII for the $\Omega = 4$, $J = 5 \leftarrow 4$ transitions differ very slightly (about 0.3 MHz lower) from the values we gave in Ref. (*4*), due to a refinement of the parameter values in the current work.

There is much further work to be done on the CoH radical. One important objective which remains is the detection of the molecule in its highest spin component, $^3\Phi_2$. The search in the far-infrared would be considerably aided by the identification of this state in the optical spectrum. To this end, we are reexamining the 449-nm band system by laser excitation spectroscopy to see if any transitions involving the $\Omega = 2$ component can be observed.

We have already mentioned that we have observed several LMR spectra of CoH in other low-lying electronic states; an example is shown in Fig. 3. We can be sure of this statement because the unmistakable hyperfine structure observed (an octet of doublets) identifies the carrier, but the Co hyperfine splittings do not conform to any of the $X\,^3\Phi$ spin components (to a very good approximation, this splitting in field units is constant for all rotational transitions within a given spin component and so is characteristic of it). Further, more systematic studies of CoH need to be made to identify the electronic states involved. Almost certainly, perturbations will be discovered which will make the analysis difficult, but a good ab initio calculation of the electronic states of CoH (*5*) should help the understanding of these results and make the experimental study more worthwhile.

It is also desirable to study the far-infrared LMR spectrum of CoD. These data, when combined with those for CoH, would permit a more reliable discussion of the perturbations between the low-lying electronic states because the strength of the couplings would be modified in the deuterated species.

ACKNOWLEDGMENT

We are very grateful to Tom Varberg for helpful comments on an earlier version of the manuscript.

RECEIVED: November 2, 1993

REFERENCES

1. B. LINDGREN AND G. OLOFSSON, *Astron. Astrophys.* **84,** 300–303 (1980).
2. P. K. CARROLL AND P. MCCORMACK, *Astrophys. J. Lett.* **177,** L33–L36 (1972).
3. P. K. CARROLL, P. MCCORMACK, AND S. O'CONNOR, *Astrophys. J.* **208,** 903–913 (1976).
4. J. M. BROWN, S. P. BEATON, AND K. M. EVENSON, *Astrophys. J. Lett.* **414,** L125–L127 (1993).
5. M. FREINDORF, C. M. MARIAN, AND B. A. HESS, *J. Chem. Phys.* **99,** 1215–1223 (1993).
6. A. HEIMER, *Z. Phys.* **104,** 448–457 (1937).
7. L. KLYNNING AND H. NEUHAUS, *Z. Naturforsch., A* **18,** 1142 (1963).
8. L. KLYNNING AND M. KRONEKVIST, *Phys. Scr.* **6,** 61–65 (1972).
9. L. KLYNNING AND M. KRONEKVIST, *Phys. Scr.* **7,** 72–74 (1973).

10. L. KLYNNING AND M. KRONEKVIST, *Phys. Scr.* **24,** 21–22 (1981).
11. R. E. SMITH, *Proc. R. Soc. London A* **332,** 113–127 (1973).
12. T. D. VARBERG, E. J. HILL, AND R. W. FIELD, *J. Mol. Spectrosc.* **138,** 630–637 (1989).
13. S. P. BEATON, K. M. EVENSON, T. NELIS, AND J. M. BROWN, *J. Chem. Phys.* **89,** 4446–4448 (1988).
14. K. LIPUS, T. NELIS, E. BACHEM, AND W. URBAN, *Mol. Phys.* **68,** 1171–1177 (1989).
15. T. J. SEARS, P. R. BUNKER, A. R. W. MACKELLAR, K. M. EVENSON, D. A. JENNINGS, AND J. M. BROWN, *J. Chem. Phys.* **77,** 5348–5362 (1982).
16. S. M. CORKERY, J. M. BROWN, S. P. BEATON, AND K. M. EVENSON, *J. Mol. Spectrosc.* **149,** 257–273 (1991).
17. J. M. BROWN, E. A. COLBOURN, J. K. G. WATSON, AND F. D. WAYNE, *J. Mol. Spectrosc.* **74,** 294–318 (1979).
18. J. M. BROWN, A. S.-C. CHEUNG, AND A. J. MERER, *J. Mol. Spectrosc.* **124,** 464–475 (1987).
19. R. A. FROSCH AND H. M. FOLEY, *Phys. Rev.* **88,** 1337–1349 (1952).
20. H. LEFEBVRE-BRION AND R. W. FIELD, "Perturbations in the Spectra of Diatomic Molecules," p. 215, Academic Press, Orlando, FL, 1986.
21. W. WELTNER, JR., "Magnetic Atoms and Molecules," pp. 345–348, Van Nostrand–Reinhold, New York, 1983.
22. E. HIROTA, "High Resolution Spectroscopy of Transient Molecules," p. 187, Springer-Verlag, Berlin, 1985.
23. M. INGUSCIO, G. MORUZZI, K. M. EVENSON, AND D. A. JENNINGS, *J. Appl. Phys.* **60,** R161–R192 (1986).
24. J. O. HENNINGSEN AND J. C. PETERSEN, *Infrared Phys.* **18,** 475–479 (1978).
25. I. MILLS, T. CVITAS, K. HOMANN, N. KALLAY, AND K. KUCHITSU, "Quantified, Units, and Symbols in Physical Chemistry," p. 92, Blackwell, Oxford, 1988.